2. M. F. Perutz, G. Fermi, B. Luisi, B. Shaanan, R. C. Liddington, *Acc. Chem. Res.* **20**, 309 (1987).
3. S. Ohnoki, Y. Mitomi, R. Hata, K. Satake, *J. Biochem.* **73**, 717 (1973); H. Furuta, M. Ohe, A. Kajita, *ibid.* **82**, 1723 (1977); P. F. Como and E. O. P. Thompson, *Aust. J. Biol. Sci.* **33**, 643 (1980); E. Chiancone, P. Vecchini, D. Verzili, F. Ascoli, E. Antonini, *J. Mol. Biol.* **152**, 577 (1981); R. C. San George and R. L. Nagel, *J. Biol. Chem.* **260**, 4331 (1985); T. A. Borgese, J. P. Harrington, D. Hoffman, R. C. San George, R. L. Nagel, *Comp. Biochem. Physiol.* **86B**, 155 (1987).
4. M. Ikeda-Saito *et al.*, *J. Mol. Biol.* **170**, 1009 (1983).
5. W. E. Royer, Jr., W. E. Love, F. F. Fenderson, *Nature* **316**, 277 (1985).
6. W. E. Royer, Jr., W. A. Hendrickson, E. Chiancone, *J. Biol. Chem.* **264**, 21052 (1989).
7. Deoxy crystals of the *Scapharca* dimer were grown from solutions of 18 mg/ml hemoglobin in 1.7 M phosphate buffer at pH 8.5 in a Bactron I anaerobic chamber (Anaerobe Systems, Santa Clara, CA). Single, diffraction-quality crystals were only obtained by using microseeding techniques [P. M. D. Fitzgerald and N. B. Madsen, *J. Cryst. Growth* **76**, 600 (1986)]. Spectra from dissolved crystals verified the deoxygenated state of the hemoglobin in these crystals. Both the deoxy and carbon monoxide crystals contain a complete dimer per asymmetric unit. As shown in Table 1, the deoxy crystals, although not isomorphous to the carbon monoxide crystals, are clearly related. In particular, the **a** and **b** unit cell axial lengths are nearly the same in both crystal forms and the deoxy c-axis length is twice 1/c* of the liganded crystals. Thus, the packing of molecules in the **ab** plane would be similar in both crystal forms. This reduces lattice effects in comparisons between the CO and deoxy crystals. Those lattice contacts that are different have minimal effects on the dimeric interface.
8. Diffraction data were collected on an AFC5R diffractometer (Molecular Structure Corporation) from deoxy crystals that had been mounted in the anaerobic chamber in thin-walled glass capillaries and sealed with mercury and DeKhotinsky cement (Thomas Scientific). The data included Friedel pairs from two crystals for reflections corresponding to Bragg spacings greater than 3.2 Å and from a third crystal used to obtain the unique data between 3.2 and 2.4 Å. An anomalous difference Patterson map [M. G. Rossmann, *Acta Crystallogr.* **14**, 383 (1961)] clearly revealed the iron positions and confirmed the approximate packing of molecules expected from comparisons with the CO structure. The orientation and position of the subunits were then refined independently against the diffraction data to an *R* value of 0.34 at 4.0 Å resolution. This molecular replacement model was used to break phase ambiguities derived from the anomalous scattering experiment. These models resolved anomalous phases [J. L. Smith and W. A. Hendrickson, in *Computational Crystallography*. D. Sayre, Ed. (Oxford Univ. Press, New York, 1982), pp. 209–222; S. Sheriff, W. A. Hendrickson, J. L. Smith, *J. Mol. Biol.* **197**, 273 (1987)] were used to calcualte a map at 3.2 Å resolution that was further improved by 13 cycles of symmetry averaging.
9. W. A. Hendrickson and J. H. Konnert, in *Computing in Crystallography*, R. Diamond, S. Ramaseshan, K. Venkatesan, Eds. (Indian Academy of Sciences, Bangalore, 1980), pp. 13.01–13.23; W. A. Hendrickson, *Methods Enzymol.* **115**, 252 (1985).
10. W. A. Hendrickson, *Acta Crystallogr.* **A35**, 158 (1979).
11. J. S. Valentine, R. P. Sheridan, L. C. Allen, P. C. Kahn, *Proc. Natl. Acad. Sci. U.S.A.* **76**, 1009 (1979); P. Stein, M. Mitchell, T. G. Spiro, *J. Am. Chem. Soc.* **102**, 7795 (1980).
12. W. S. Caughey, C. H. Barlow, J. C. Maxwell, J. A. Volpe, W. J. Wallace, *Ann. N.Y. Acad. Sci.* **244**, 1 (1975); C. H. Barlow, J. C. Maxwell, W. J. Wallace, W. S. Caughey, *Biochem. Biophys. Res. Commun.* **55**, 91 (1973).
13. G. K. Ackers, *Biophys. J.* **32**, 331 (1980).
14. F. C. Mills and G. K. Ackers, *Proc. Natl. Acad. Sci. U.S.A.* **76**, 273 (1979).
15. We thank F. Smith for discussions about anaerobic crystallizations and suggesting the use of the Bactron I anaerobic chamber and S. Hubbard and H.-E. Aronson for computer programs. The atomic coordinates and diffraction data are being deposited in the Brookhaven Protein Data Bank. This work was supported in part by a grant for the National Science Foundation (DMB 87-17570).

1 March 1990; accepted 5 June 1990

Molecular Structure of Charybdotoxin, a Pore-Directed Inhibitor of Potassium Ion Channels

WALTER MASSEFSKI, JR., ALFRED G. REDFIELD, DENNIS R. HARE, CHRISTOPHER MILLER

The three-dimensional structure of charybdotoxin, a high-affinity peptide blocker of several potassium ion channels, was determined by two-dimensional nuclear magnetic resonance (2-D NMR) spectroscopy. Unambiguous NMR assignments of backbone and side chain hydrogens were made for all 37 amino acids. The structure was determined by distance geometry and refined by nuclear Overhauser and exchange spectroscopy back calculation. The peptide is built on a foundation of three antiparallel β strands to which other parts of the sequence are attached by three disulfide bridges. The overall shape is roughly ellipsoidal, with axes of approximately 2.5 and 1.5 nanometers. Nine of the ten charged groups are located on one side of the ellipsoid, with seven of the eight positive residues lying in a stripe 2.5 nanometers in length. The other side displays three hydrophobic residues projecting prominently into aqueous solution. The structure rationalizes several mechanistic features of charybdotoxin block of the high-conductance Ca^{2+}-activated K^+ channel.

AMONG THE NEUROTOXINS PRESENT in the venoms of buthid scorpions is a family of peptides that specifically inhibit certain K^+-specific ion channels found in electrically excitable membranes (*1, 2*). Of these peptides, charybdotoxin (CTX) is the best studied at the mechanistic and biochemical levels (*3, 4*). It is known (*5*) that CTX inhibits its K^+ channel target by binding to the externally facing ion entryway and physically blocking the permeation of K^+ ions. Because of this simple mode of action, CTX has proven valuable as a probe of the molecular nature of K^+ channels, including the size of the external channel "mouth" and the disposition of charges on the channel protein surface (*5*). Our ability to use CTX in this way would be greatly enhanced by a knowledge of the peptide's 3-D structure. Since the toxin is only a minor component of venom proteins in even the richest known source, it is not feasible at present to undertake crystallization studies that would lead to structure determination by x-ray crystallography. However, the peptide's small size (37–amino acid residues), known primary sequence, and conformational rigidity resulting from its three disulfide bonds make it an appropriate target for attack by 2-D NMR methods. In this report, we describe the use of this technique to determine the solution structure of CTX.

The 1-D ^1H NMR spectra of a sample of CTX at pH 4.0 in both D_2O and H_2O (Fig. 1A) demonstrate that the sample produces high-quality peaks suitable for 2-D NMR procedures (*6*). A homonuclear Hartmann-Hahn transfer (HOHAHA) experiment (Fig. 1B), which yields a map of through-bond couplings, illustrates the well-resolved cross peaks in the Hα-Hβ region. Assignment of individual protons to the resonance lines was done in two stages (*7*). First, side chains were assigned as far as possible from the scalar coupling patterns of correlation spectroscopy (COSY), HOHAHA, and double-quantum experiments. This process was straightforward for aromatic residues, since each (Phe, Trp, Tyr, and His) occurs only once in CTX. The methyl-containing residues were easily divided into amino acid types, since only one Leu, two Val, and four Thr residues are present in CTX. Glycine-26 was identified by a single NH-Hα remote peak in the double-quantum experiment. Serines were identified from the rest of $\alpha\beta_2$ spin systems by their unusually downfield β protons (Fig. 1B). The unique glutamate

W. Massefski, Jr., Graduate Department of Biochemistry, Brandeis University, Waltham, MA 02254.
A. G. Redfield, Graduate Department of Biochemistry and Physics, Brandeis University, Waltham, MA 02254.
D. R. Hare, Hare Research, Inc., Woodinville, WA 98072.
C. Miller, Howard Hughes Medical Institute, Graduate Department of Biochemistry, Brandeis University, Waltham, MA 02254.

was identified as the only $\alpha\beta_2\gamma$ spin system in which the $\beta\gamma$ cross peak shifted appreciably when the pH was changed from 7.0 to 4.0. The ring δ protons of Phe[2] and Tyr[36] both give nuclear Overhauser and exchange spectroscopy (NOESY) cross peaks to their respective β protons to identify these unique residues. The side chain amides of Asn[4], Gln[18], Asn[22], and Asn[30] were identified from the H_2O COSY and were connected to their respective β protons from direct peaks in the double-quantum spectrum. The Arg NH protons were identified from their strong cross peak to water in a selective-observe H_2O NOESY experiment, and the Lys amino protons gave cross peaks to their ε side chain protons in the double-quantum experiment. Complete side chain assignments for the four Lys and three Arg in CTX were accomplished from scalar coupling information obtained in the experiments listed above.

In the second phase of assigning resonance lines to individual protons, we used the unique residues Phe[2], Glu[12], Leu[20], Gly[26], and Tyr[36] as landmarks for the sequential assignment process. In this process, each NH-Hα intraresidue connection was established by the combination of H_2O COSY, HOHAHA, and double-quantum experiments, and the Hα-Hβ intraresidue connections were established from D_2O HOHAHA experiment. The connection from amide to β proton was checked with an H_2O HOHAHA experiment in which selective-pulse detection was used. Finally the interresidue sequential connectivities (Fig. 2) were made from the H_2O NOESY data by using strong amide to α, β, or adjacent amide cross peaks to make the sequential assignments (*8*). With the use of the above landmarks, this process produced connectivities for the following sequences of residues: pyGlu[1] to Cys[7], Thr[8] to Ser[10], Lys[11] to Cys[17], Arg[19] to Thr[23], Ser[24] to Asn[30], Lys[31] to Lys[32], Arg[34] to Cys[35], and Tyr[36] to Ser[37]. The remaining two residues, Gln[18] and Cys[33], were easily distinguished because they have different scalar coupling patterns. The sequential connectivities were consistent with the amino acid types identified from the scalar coupling experiments.

The sequence-specific assignments led immediately to conclusions about the secondary structure of CTX, based mostly on NOESY cross peaks obtained in D_2O and H_2O solution. The D_2O NOESY gave Hα-Hα cross peaks between residues 2 and 13 and between 14 and 26; the H_2O NOESY gave NH-Hα cross peaks between residues 27 and 14 and between 15 and 26; these couplings lead directly to the conclusion that there is a short, three-strand antiparallel β sheet in CTX near these residues. The presence of strong NH-NH cross peaks between residues 21, 22, and 23 indicates that these residues are involved in a type Iβ turn.

The distance geometry program DSPACE (*9*) was used for the structure determination. Methylene atoms were included explicitly in the calculations, and standard covalent geometry was preserved throughout. We used 103 distance constraints (42 intraresidue, 36 sequential, and 25 long range) to generate structures consistent with the qualitative structure predictions drawn above. The structures were determined exclusively from NOE and disulfide bond constraints; hydrogen bonds and dihedral bond angles were not used, although the NH-Hα scalar coupling constants were consistent with the resulting structures. NOE intensities were calibrated against cross peaks of the unique Trp ring in 100-, 150-, 300-, and 600-ms NOESY experiments. Back calculation of the NOESY spectra from each structure was used to adjust the distance estimates, add negative constraints, and confirm the identity of ambiguous NOEs. The final set of five structures satisfied all NOE constraints within 0.1 Å. Backbone atom and all-atom superpositions of these structures had root-mean-square deviations of less than 0.9 $Å^2$ and 1.5 $Å^2$, respectively.

The disulfide bonds used in this work between residues 7 and 28, 13 and 33, and 17 and 35, were taken from enzymatic digestion studies (*10*) and are consistent with the assignments and calculations we report. The use of incorrect disulfide pairings made it impossible to generate well-refined structures. We confirmed that our sample of CTX contained three disulfide bridges by using fast atom bombardment mass spectroscopy. Several aspects of additional NMR data are consistent with the calculated structures. First, the somewhat downfield chemical shifts of β protons in the region from Lys[32] to Cys[35] are consistent with the high positive charge density found in this region. Second, measurements of amide proton-exchange longitudinal relaxation time indicate that the fast-relaxing amides are exposed to solvent in our structure. Finally, the longitudinal relaxation times of the Phe[2] ring protons are among the longest in the molecule, indicating that this ring rotates rapidly and is solvent exposed.

The polypeptide backbone folding pattern of the final structure is shown in Fig. 3. The precision of the structure determination was uniform throughout the polypeptide

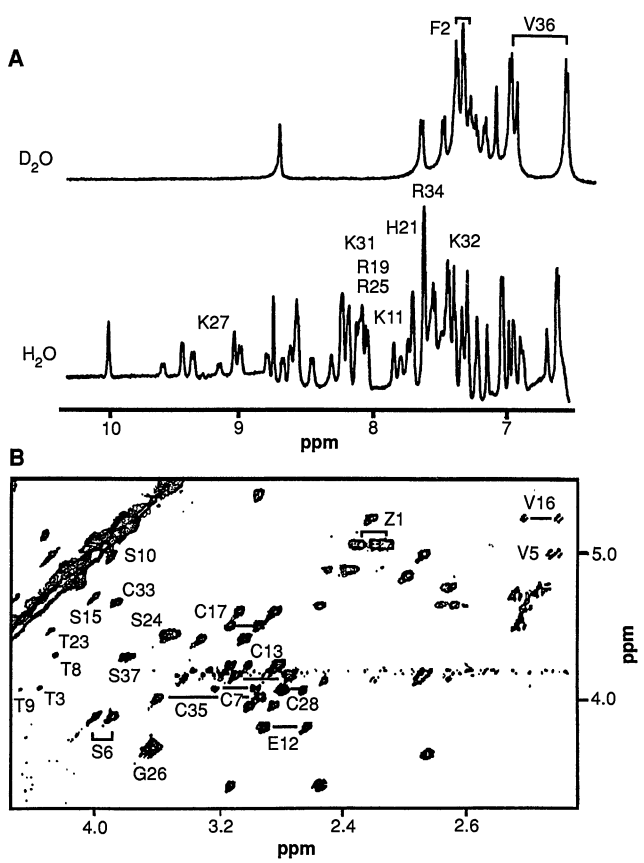

Fig. 1. Proton NMR spectra of CTX. NMR spectra of purified CTX (*4*, *11*) dissolved in 175 mM NaCl, 30 mM sodium acetate, pH 4.0, were collected on a custom-built spectrometer operating at 500 MHz. (**A**) Downfield 1-D spectra in D_2O (upper trace) and H_2O (lower trace). Peaks common to both spectra are from nonexchangeable aromatic ring protons; peaks seen only in the H_2O spectra are from backbone amides and protons bonded to nitrogen atoms on Lys, Arg, Asn, and Gln side chains. The D_2O spectrum was obtained by signal averaging 300 transients, with short pulse observation, 2-s recycle time, and quadrature detection. The H_2O spectrum was obtained with a 214 observation pulse. (**B**) HOHAHA spectrum obtained in D_2O. The region of the spectrum shown contains cross peaks between Hα protons (vertical axis) and other side chain protons (methyl, β, γ, and such, horizontal axis). The spectrum was taken with a 30-ms spin lock and 1-ms trim pulses (*16*), collecting 960 and 2048 points in the t_1 and t_2 dimensions. Transforms were calculated by standard methods (*17*). The Hα to Hβ cross peaks of all Glu, Thr, Ser, and Cys residues are labeled, as well as the secondary Hα to methyl cross peaks of both Val residues (*18*).

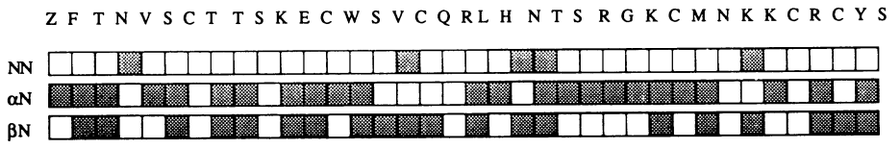

Fig. 2. Sequential NOE connectivities in CTX. Shaded regions indicate the interresidue NOEs observed.

backbone. Three antiparallel β strands, identified clearly from Hα-Hα couplings, provide a basic foundation on which the molecule is built. This small β sheet is formed from residues 1 to 3, 12 to 15, and 25 to 27. A type I β turn (residues 20 to 23) separates the second and third strands of the sheet, and a type II β turn (residues 29 to 32) leads out of the sheet into the COOH-terminal region. Two of the three disulfide bonds (13 to 33 and 17 to 35) connect the central β strand to the COOH-terminal region, which lies on the β sheet. The third disulfide bond (7 to 28) connects the first and third intrastrand loops to each other. These disulfides are apparently essential for maintaining the toxin conformation, since reduction results in a complete loss in blocking activity (*4*). No α helix is present in this structure.

Two space-filled views ("front" and "back") of the molecule, now with side chain residues included, are shown in Fig. 4. The toxin resembles a lumpy prolate ellipsoid, with axes of 2.5 and 1.5 nm long. The distribution of charged residues is striking. Of the eight positive charges (shown in blue), seven are found on the same side of the molecule along a well-defined stripe on one face; one of these, Arg^{19}, is located at the top of the molecule. The two negatively charged groups (red), Glu^{12} and the terminal carboxylate, are also found on this "polar face." All of the strongly hydrophobic residues (brown) are found on the opposite side. Particularly noticeable are the two aromatic residues Phe^2 and Tyr^{36}, which project off this nonpolar face into aqueous solution. The other hydrophobic residues, Val^5, Trp^{14}, Val^{16}, and Leu^{20}, are also located on this side of the structure, and only a single charged residue, Arg^{25}, is found on this face. The toxin is too small to have a hydrophobic core or even a well-defined interior; indeed, every one of its amino acid units is exposed to solvent, either in its side chain or backbone groups.

Our proposed structure fits well with the known mechanism of CTX action on K^+ channels, which has been extensively studied in high-resolution electrophysiological measurements of single CTX molecules blocking single channels. The striking clustering of cationic residues on one face of the toxin brings to mind the strong ionic strength dependence of CTX block, which had pointed toward the functional importance of positively charged residues (*11*). For the high-conductance Ca^{2+}-activated K^+ channel, binding of CTX to the external channel "mouth" literally plugs up the K^+ conduction pore (*5*). Since this channel's conduction pathway is also physically blocked by alkyl ammonium and guanidinium cations (*12*), we speculate that one of the positive residues on the toxin may block the narrower part of the pore, while the rest of the molecule makes stabilizing interactions in the wider part of the pore mouth. Some of these stabilizing interactions may be electrostatic, since Lys acylation reduces the toxin affinity greater than 100-fold (*4*).

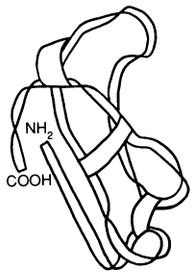

Fig. 3. Backbone folding pattern of the CTX structure. This ribbon representation of the polypeptide backbone folding pattern of CTX shows the NH_2- and COOH-termini as well as the three disulfide bridges (connecting residues 7 and 28, 13 and 33, and 17 and 35), which are indicated by short, wide ribbons.

The known biochemistry of CTX suggests that hydrophobic residues are also involved in the specific binding of toxin to channel protein. For instance, chymotrypsin removes the two NH_2-terminal amino acids by cleaving CTX at Phe^2 (*13*), a residue which, in spite of its hydrophobic nature, directly protrudes into aqueous solution in our structure. This treatment lowers the CTX binding affinity about 80-fold (*4*), mainly by increasing the toxin's off-rate. Similarly, monoiodination of Tyr^{36}, a modification that would sterically prevent the phenol ring from lying flat on a hydrophobic surface, vastly lowers the toxin affinity (*2*). Both of these biochemical insults are directed towards prominent surface residues on the molecule's nonpolar face (Fig. 4), which we imagine makes specific contacts with the K^+ channel mouth.

The segregation of polar and nonpolar faces in this structure is especially interesting, since the toxin receptor is very likely a structure with high symmetry. Current evidence suggests that voltage-dependent K^+ channels are built as tetramers of identical subunits arranged around a central pore (*14*). If the toxin fits snugly into the channel mouth, then each channel monomer must provide receptor sites for both the charged and nonpolar faces of the toxin. These sites on the channel wall must be aligned so that when one side of the toxin contacts hydrophobic receptor sites on one monomer, the other side contacts polar groups on a different, but chemically identical, monomer. Although more extreme in detail, this situation is similar in many respects to the binding of 2,3-bis-phosphoglycerate to the tetrameric interface in hemoglobin. This picture requires that the external mouth of the channel is 1.5 to 2 nm wide and at least 2 nm deep; these are reasonable dimensions if the mouth of the acetylcholine receptor (2.5 nm by 6 nm) is at all representative of ion channels in general (*15*).

The proposed structure of CTX immediately suggests further experiments to assess the importance of specific residues in toxin binding. Positively charged residues contribute strongly to binding to the K^+ channel mouth, which carries functionally important negative charges (*11*). At present we can only speculate about which of the eight basic residues may be directly involved in occluding the K^+ conduction pathway; for instance, does the obvious candidate, Arg^{19}, which projects off the "top" of the molecule, really function as a tethered pore blocker, with other groups on CTX critical to the specificity and affinity of the interaction? High-level expression of a synthetic gene for

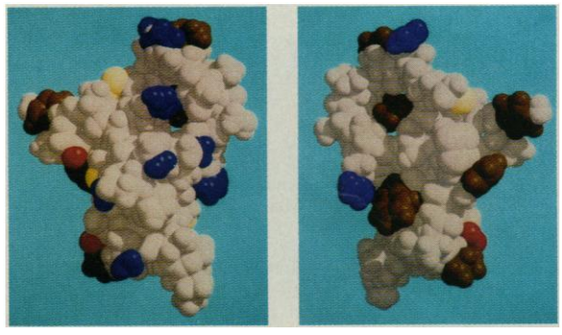

Fig. 4. Location of functional groups on CTX. Space-filling representations of CTX, showing positions of positively charged residues in blue, negative charges in red, and hydrophobic residues (Phe^2, Val^5, Trp^{14}, Val^{16}, Leu^{20}, and Tyr^{36}) in brown. (**Left**) "Front" view of molecule with charged face visible. (**Right**) "Back" view, with molecule rotated 180° about its long axis.

CTX will allow these ideas to be tested through site-directed mutagenesis, and the structure of such mutants can be routinely determined by 2-D NMR spectroscopy.

REFERENCES AND NOTES

1. E. Moczydlowski, K. Lucchesi, A. Ravindran, *J. Membr. Biol.* **105**, 95 (1988); E. Carbone, G. Prestipino, L. Spadavecchia, F. Franciolini, L. D. Possani, *Pflugers Arch.* **408**, 423 (1987).
2. K. Lucchesi, A. Ravindran, H. Young, E. Moczydlowski, *J. Membr. Biol.* **109**, 269 (1989).
3. C. Miller, E. Moczydlowski, R. Latorre, M. Phillips, *Nature* **313**, 316 (1985); G. Gimenez-Gallego *et al.*, *Proc. Natl. Acad. Sci. U.S.A.* **85**, 3329 (1988).
4. C. Smith, M. Phillips, C. Miller, *J. Biol. Chem.* **261**, 14607 (1986).
5. R. MacKinnon and C. Miller, *J. Gen. Physiol.* **91**, 335 (1988); C. Miller, *Neuron* **1**, 1003 (1988); R. MacKinnon, R. Latorre, C. Miller, *Biochemistry* **28**, 8087 (1989).
6. All 2-D NMR experiments were performed by collecting 2048 (t_2) by 960 (t_1) points: the data were zero-filled twofold in each dimension to give a Fourier-transformed data set containing 2048 by 1024 points. Experiments were done with 32 to 96 acquisitions per t_1 point, and data were processed with moderate convolution difference in both dimensions. COSY experiments used a 2-s relaxation delay, and H_2O COSY used saturation of the H_2O resonance during the delay. D_2O HOHAHA was performed with a 32-ms mixing period, 1-ms trim pulses, and a 2-s relaxation delay. H_2O HOHAHA experiments used a selective observation pulse and a spoil pulse after the 48-ms mixing period (with 1-s relaxation delay). The double-quantum experiment was performed in H_2O with a 22-ms coherence delay, and water was saturated for 0.6 s of the 1-s relaxation delay period. The D_2O NOESY was performed with 300-ms mixing time and a 2-s relaxation delay. H_2O NOESY experiments used mixing periods of 100, 150, 300, and 600 ms.
7. K. Wuthrich, *NMR of Proteins and Nucleic Acids* (Wiley, New York, 1986).
8. W. S. Englander and J. Wand, *Biochemistry* **26**, 5953 (1987).
9. M. F. Summers, T. L. South, B. Kim, D. R. Hare, *ibid.* **29**, 329 (1990).
10. M. L. Garcia, E. E. Sugg, J. P. Reuben, A. A. Patchett, G. J. Kaczorowski, *Biophys. J.* **57**, 118a (1990).
11. C. Anderson, R. MacKinnon, C. Smith, C. Miller, *J. Gen. Physiol.* **91**, 317 (1988); R. MacKinnon and C. Miller, *Biochemistry* **28**, 8092 (1989).
12. A. Villarroel, O. Alvarez, A. Oberhauser, R. Latorre, *Pflugers Arch.* **413**, 118 (1989); C. Vergara, E. Moczydlowski, R. Latorre, *Biophys. J.* **45**, 73 (1984).
13. C. Smith, thesis, Brandeis University, Waltham, MA (1988).
14. W. A. Catterall, *Science* **242**, 50 (1988); L. Y. Jan and Y. N. Jan, *Cell* **56**, 13 (1989).
15. C. Toyoshima and N. Unwin, *Nature* **336**, 247 (1988).
16. A. Bax and D. G. Davis, *J. Magn. Reson.* **65**, 355 (1985).
17. D. J. States, R. A. Haberkorn, D. J. Ruben, *ibid.* **48**, 286 (1982).
18. Abbreviations for the amino acid residues are: A, Ala; C, Cys; D, Asp; E, Glu; F, Phe; G, Gly; H, His; I, Ile; K, Lys; L, Leu; M, Met; N, Asn; P, Pro; Q, Gln; R, Arg; S, Ser; T, Thr; V, Val; W, Trp; Y, Tyr; and Z, pyGlu.
19. The atomic coordinates of the structure shown in Fig. 4 have been deposited in the Brookhaven Protein Data Bank. We thank D. Ringe for use of a Silicon Graphics computer, I. Papayannopoulos of the MIT mass spectroscopy facility for performing FAB-MS of CTX, and H. M. Massefski for drawing Fig. 3. Supported by NIH grants GM-31768 (C.M.) and GM-20168 (A.G.R.). The FAB-MS facility is supported by the NIH Division of Research Resources Grant RR0031.

20 March 1990; accepted 14 June 1990

The Energetic Cost of Limbless Locomotion

MICHAEL WALTON, BRUCE C. JAYNE, ALBERT F. BENNETT

The net energetic cost of terrestrial locomotion by the snake *Coluber constrictor*, moving by lateral undulation, is equivalent to the net energetic cost of running by limbed animals (arthropods, lizards, birds, and mammals) of similar size. In contrast to lateral undulation and limbed locomotion, concertina locomotion by *Coluber* is more energetically expensive. The findings do not support the widely held notion that the energetic cost of terrestrial locomotion by limbless animals is less than that of limbed animals.

SPECIES WITH REDUCED LIMBS OR NO limbs and elongate bodies have evolved independently from limbed antecedents in several groups of vertebrates: salamanders, caecilians, amphisbaenians, lizards, and snakes (*1*). An important factor proposed to explain the evolution of limblessness is its presumptively low energetic cost, such that energetic expenditure during locomotion by limbless animals is expected to be less than that of limbed animals of similar size (*1, 2*). Biomechanical arguments advanced in support of the low energetic cost of limbless locomotion include no costs associated with vertical displacement of the center of gravity (*1, 3, 4*), no costs to accelerate or decelerate limbs (*3*), and low cost for support of the body (*1*). A preliminary study, published only as an abstract, reported that the energetic cost of locomotion of the garter snake (*Thamnophis sirtalis*) was only 30% of that predicted for a quadrupedal lizard of similar size (*5*). Although that study was preliminary, it has been widely cited in review articles (*1–3, 6, 7*) and textbooks (*4, 8*) in support of mechanical arguments for the low cost of limbless locomotion. We sought to test the generality of these conclusions by examining the energetic cost of locomotion in a snake, the black racer (*Coluber constrictor*).

A snake may utilize a variety of locomotor modes, depending on both speed and surface encountered (*4, 9–11*). Lateral undulation and concertina locomotion are two common modes that use lateral vertebral movements to generate propulsive forces. During lateral undulation on the ground, snakes move along an approximately sinusoidal trajectory. Bends in the body contact with the substrate and push posteriorly on projections from the ground, propelling the body forward. All parts of the body move simultaneously with the same overall speed, while forward and lateral components of velocity change as a result of the sinusoidal trajectory (*10, 11*). Snakes moving with lateral undulation experience only sliding contact with the ground (*4, 12*). In narrow passageways such as tunnels, snakes often perform concertina locomotion exclusively (*4*). Snakes performing concertina locomotion stop periodically, and certain parts of the body are moved forward while others maintain static contact with the ground. In passageways, snakes alternately press themselves against the sides by forming a series of bends and then extend themselves forward from the region of static contact (*4, 13*). In comparison to lateral undulation, concertina locomotion involves higher momentum changes (*4*), resistance due to static (as well as sliding) friction (*4*), and usually slower forward speed (*11*) and, therefore, probably entails higher energetic costs.

Although these considerations logically suggest differential costs of the two locomotor modes, only if we directly determine the metabolic rates of moving animals can these be verified and compared to anticipated values for limbed animals. In the current study, we measured energy expenditure as the rate of oxygen consumption of snakes at rest ($\dot{V}O_{2\ rest}$), in the moments just before locomotory exercise ($\dot{V}O_{2\ pre\text{-}ex}$), and during locomotion at several speeds (0.2 to 1.0 km hour^{-1} for lateral undulation, 0.06 to 0.14 km hour^{-1} for concertina locomotion) on motorized treadmills (*14, 15*). Endurance, measured as time sustained on tread, as a function of speed and locomotor mode was also determined (*16*). Videotapes were used to verify locomotor mode and to correlate frequency of movement with energy expenditure. By dividing oxygen consumption by frequency of movement, we estimated energetic costs of single cycles of lateral undulatory and concertina movement.

The metabolic response of $\dot{V}O_2$ to speed in *Coluber constrictor* [mass = 102.8 ± 6.1 (SE) g, n = 7] locomoting by lateral undulation is similar to that observed in many terrestrial vertebrates with limbs (*17*): $\dot{V}O_2$ increases as a linear function of speed (*18*) throughout the range of sustainable speeds (0.2 to 0.5 km hour^{-1}), above which $\dot{V}O_2$ is constant and endurance decreases (speeds greater than 0.5 km hour^{-1}) (Fig. 1, A and B). Oxygen consumption also increased as a

Department of Ecology and Evolutionary Biology, University of California, Irvine, CA 92717.